Title: “Metformin Impairs Intestinal Fructose Metabolism”

Authors:
Wenxin Tong[1], Sarah A. Hannou[1,3], Ashot Sargsyan[1], Guo-Fang Zhang[1,2], Paul A. Grimsrud[1,2], Inna Astapova[1,2,3], and Mark A. Herman[1,2,3]

1 Duke Molecular Physiology Institute, Duke University, Durham, North Carolina, USA;
2 Division of Endocrinology, Metabolism, and Nutrition, Duke University, Durham, North Carolina, USA;
3 Division of Endocrinology, Diabetes, and Metabolism, Baylor College of Medicine, Houston, Texas, USA

Corresponding Author:
Mark A. Herman; Division of Endocrinology, Diabetes, and Metabolism, Baylor College of Medicine, Houston, Texas, USA
mark.herman@bcm.edu

Abstract

Objective: To investigate the effects of metformin on intestinal carbohydrate metabolism *in vivo*.

Method: Male mice preconditioned with a high-fat, high-sucrose diet were treated orally with metformin or a control solution for two weeks. Fructose metabolism, glucose production from fructose, and production of other fructose-derived metabolites were assessed using stably labeled fructose as a tracer.

Results: Metformin treatment decreased intestinal glucose levels and reduced incorporation of fructose-derived metabolites into glucose. This was associated with decreased intestinal fructose metabolism as indicated by decreased enterocyte F1P levels and diminished labeling of fructose-derived metabolites. Metformin also reduced fructose delivery to the liver. Proteomic analysis revealed that metformin coordinately down-regulated proteins involved carbohydrate metabolism including those involved in fructolysis and glucose production within intestinal tissue.

Conclusion: Metformin reduces intestinal fructose metabolism, and this is associated with broad-based changes in intestinal enzyme and protein levels involved in sugar metabolism indicating that metformin's effects on sugar metabolism are pleiotropic.

Key words

Metformin, glucose production, fructose metabolism, isotope-tracing metabolomics, proteomics

45 **Highlights**

46 - Metformin decreases intestinal fructose absorption, metabolism, and fructose
47 delivery to the liver.
48 - Metformin reduces intestinal glucose production from fructose-derived
49 metabolites.
50 - Metformin reduces protein levels of multiple metabolic enzymes involved in
51 fructose and glucose metabolism in intestinal tissue.

52

53 **Introduction**

54 Metformin is a first-line anti-diabetic drug and the most widely prescribed oral anti-
55 hyperglycemic worldwide [1]. Beneficial effects of metformin have also been suggested
56 for people with obesity [2], non-alcohol fatty liver disease [3], Alzheimer's disease [4], and
57 some cancers [5; 6]. Even though metformin has been investigated intensively for
58 decades, the target organ(s) and the underlying mechanism of metformin's beneficial
59 effects remain controversial.

60 Metformin's anti-diabetic effects are often attributed to its ability to reduce
61 endogenous glucose production [7; 8]. Because the liver is the major site of
62 gluconeogenesis in mammals, most studies have focused on metformin's effects on liver
63 tissue [9]. However, the role of liver in metformin's actions is receiving more scrutiny as
64 therapeutic doses of metformin may not produce sufficient concentrations of metformin in
65 hepatocytes to mediate its observed systemic effects [8; 10]. In contrast with liver,
66 metformin is highly concentrated in intestinal tissue [11; 12]. In intestinal tissue, metformin
67 may achieve concentrations that are 100 to 300-fold higher than circulating plasma levels,
68 and ~ 2-10-fold higher than that in the liver [11; 12]. This suggests that metformin has the
69 potential to have outsized impact on intestinal function to regulate systemic glucose
70 homeostasis [13]. Metformin may regulate glycemia through effects on the intestine via
71 multiple mechanisms. For instance, a recent study showed that metformin's glucose-
72 lowering effect is mediated through activating the PEN2-directed lysosomal AMPK
73 pathway in intestinal tissue and not in liver [14]. Additionally, multiple studies in both
74 humans and preclinical models using a F18- fluorodeoxyglucose (F18-FDG) tracer
75 indicate that metformin enhances glucose uptake in the colon and possibly the small
76 intestine [13; 15; 16]. Recent studies from our group and others demonstrated that
77 fructose is metabolized at high rates in intestinal tissue and contributes to intestinal
78 glucose production [17; 18]. In this study, using fructose to assess enterocyte metabolic
79 function and as a gluconeogenic tracer, we show that short-term treatment of mice with
80 metformin impairs intestinal carbohydrate metabolism and reduces intestinal glucose
81 production adding to the mechanisms by which metformin impacts systemic glucose
82 homeostasis.

83

Methods

Materials:

Metformin (hydrochloride) was purchased from Cayman Chemical (No. 13118). D-Fructose was purchased from VWR international (VWRV0226). [U-^{13}C]-fructose, and [U-^{13}C]-fructose-6-phosphate (M6-F6P) were purchased from Cambridge Isotope Labs (CLM-1553-PK, and CLM-8616 respectively). Norvaline and D-[1,6-$^{13}C_2$]-fructose (M2-fructose) were purchased from Sigma-Aldrich (53721 and 587613 respectively).

Animals:

All animal experiments were approved by Duke Institutional Animal Care and Use Committee. 17-18 weeks old wild-type C57/BL6J (Stock# 000664) male mice were purchased from The Jackson Laboratory and maintained in a pathogen free vivarium at Duke University. All animals were maintained at ~ 22°C on a 12-hour light-dark cycle (6 AM to 6 PM) and adapted for at least one week before any experimental procedure or intervention. Within experiments, mice were divided randomly into either water control or metformin treatment groups. To prepare the metformin oral-gavage solution, 500 mg metformin was dissolved in 20 mL sterile water and aliquoted into 14 vials stored at 4 °C. After pretreatment of all mice with 1 week of high-fat, high-sucrose diet (45% fat, 20% sucrose, Research Diet, D12451i), we randomly distributed mice to two groups and orally gavaged water or metformin solutions at a dose of 10 μL/g body weight. After two weeks of metformin or water administration, an i.p. glucose tolerance test (GTT) was conducted. Two days after the i.p. GTT was performed, mice were sacrificed 30 minutes after fructose gavage (1:1 mixture of unlabeled fructose and [U-^{13}C]-fructose). Unless otherwise noted, all procedures including oral gavage and body weight measurement were performed at 9:30 AM. Euthanasia after fructose gavage was performed at 2 PM, 5 hours after food removal at 9 AM.

Glucose tolerance test:

Animals were fasted for 5 hours starting at 9 AM. At 2PM, animal body weight was measured, and sterile glucose solution was injected intraperitoneally at a dose of 1.5 g/Kg

114 body weight. Glycemia was measured using a drop of blood drawn from a nicked tail vein
115 via glucometer (Bayer Contour) at 0, 15, 30, 60, 90, and 120 minutes after injection.
116
117 Animal euthanasia and sample/tissue harvest:
118 Animals were euthanized under isoflurane anesthesia 30 minutes after fructose
119 gavage (1:1 mixture of unlabeled fructose and [U-^{13}C]-fructose at 4g/Kg body weight).
120 Mice were anesthetized under continuous oxygen following the guidelines recommended
121 by the Duke Institutional Animal Care and Use Committee. Once deep anesthesia was
122 confirmed by a toe pinch, blood samples from the tail vein were harvested. Laparotomy
123 was subsequently performed, and the portal vein was exposed. Clean scissors were used
124 to make a small incision in the portal vein, and blood (200 μL) was extracted using a 1
125 mL syringe from the peritoneal cavity and transferred to an EDTA-coated blood collection
126 tube (Sarstedt, 16.440.100). The liver and intestine were removed from the abdominal
127 cavity. Liver tissue was snap frozen in liquid nitrogen. The small intestine extending from
128 0.5 cm distal to the end of the stomach and extending to 0.5 cm proximal to the cecum
129 was excised, flushed with ice-cold PBS and snap frozen in liquid nitrogen.
130
131 Gas chromatography-mass spectrometry (GC/MS):
132 Plasma was prepared from collected blood by centrifugation at 2,000 g, 4°C for 15
133 minutes. Tissue samples were powdered under liquid N_2. 0.2 mM 2-Deoxy-D-glucose
134 (2DG), 0.2 mM M2-fructose, 0.1 nM M6-F6P or 0.1 mmol norvaline was added to 10 μL
135 plasma samples or 10 mg powdered tissue samples as an internal standard for the
136 measurement of glucose, fructose or TCA cycle intermediates respectively. After that,
137 400 μL MeOH, 400 μL ddH2O, and 400 μL chloroform were added sequentially and briefly
138 vortexed after each addition. After centrifugation at 12,000 g for 15 minutes, supernatants
139 were collected and dried under nitrogen.
140 Relative quantification and enrichment measurements for glucose, glycerate, F1P,
141 and GA3P: Dried sample residues were derivatized with methoxylamine hydrochloride
142 and trimethylsilyl (TMS) sequentially. Specifically, 25 μL of methoxylamine hydrochloride
143 (2% (w/v) in pyridine) was added to the dried residues and incubated for 90 minutes at
144 40°C before the addition of 35 μL of TMS and incubation for 30 minutes at 60°C. The

145 samples were then centrifuged for 2 minutes at 12,000 g and the supernatants of
146 derivatized samples were transferred to GC vials for further analysis.
147 Absolute quantification of fructose: the dried residues were derivatized with
148 methoxylamine hydrochloride and propionic anhydride sequentially adapted from a
149 previously described method [19]. 25 µL of methoxylamine hydrochloride (2% (w/v) in
150 pyridine) was added to the dried residues and incubated for 60 minutes at 70°C. After
151 centrifugation for 2 minutes at 12,000 g, 50 µL propionic anhydride was added and
152 incubated for 30 minutes at 60°C prior to another round of drying under nitrogen. The
153 dried residues were resuspended with 55 µl pure ethyl acetate and transferred to GC vials
154 for analysis.
155 Relative quantification and enrichment measurements of TCA cycle intermediates:
156 Dried residues were derivatized with methoxylamine hydrochloride and
157 tertbutyldimetheylchloros (TBDMS) sequentially as previously described [3]. 25 µL of
158 methoxylamine hydrochloride (2% (w/v) in pyridine) was added to the dried residues and
159 incubated for 90 minutes at 40°C before the addition of 35 µL of TBDMS and incubation
160 for 30 minutes at 60°C. The samples were then centrifuged for 2 minutes at 12,000 g and
161 the supernatants of derivatized samples were transferred to GC vials for further analysis.
162 GC/MS analysis was conducted using an Agilent 7890B GC system and Agilent
163 5977A Mass Spectrometer. 1 µL of the derivatized sample was injected into the GC
164 column. The GC temperature gradient started at 90°C, increased to 260°C at the speed
165 of 9°C per minute and further increased to 290 °C at the speed of 30°C per minute. Then
166 the temperature was held at 290°C for 5 minutes with a run time of 24.9 minutes.
167 Ionization was conducted by EI at 70 eV with Helium flow at 1 mL/min. Temperatures of
168 the source, the MS quad, the interface, and the inlet were maintained at 230°C, 150°C,
169 280°C, and 250°C, respectively. Mass spectra were recorded in mass scan mode from
170 m/z 50 to 700. The levels of metabolites were calculated based on the area of the peak
171 at its specified retention time. Total ion counts (A.U.) of metabolites were assessed as
172 the sum of its isotopologues and normalized to their specific standards as detailed above
173 and below.
174
175 Stable Isotope Analysis and Average Carbon-13 Label Incorporation Rates:

176 Isotopologues containing 0, 1, to n heavy atom(s) in a molecule were referred as
177 M+0, M+1, to M+n respectively. The retention times of individual metabolites and their
178 isotopomers are described in Supplementary Table 1. Isotope enrichment and labeling
179 analysis in this study were corrected for natural isotope distribution as previously
180 described [20; 21]. Specifically, the stable isotope enrichment of each metabolite in
181 plasma and tissue samples was corrected based on the natural isotope distribution
182 measured in the same type of sample treated without labeled molecules. For example,
183 the natural isotope distribution matrix of individually measured metabolites in the blood
184 samples were experimentally determined by assaying and averaging the blood samples
185 from animals who had not received any treatment with isotopically labeled sources.
186 The average carbon-13 incorporation was calculated according to the equation as
187 previously described in reference (18). Specifically, n_{M+i} refers to the number of ^{13}C
188 carbons in the isotopomer (M+i). For example, n = 0 for M+0, n = 1 for M+1, and n = 2 for
189 M+2, and so on. "A" refers to the corresponding percentage abundance of the isotopomer.
190 N refers to the total carbon number, which for glucose, N = 6.
191

192 $$Average\ C13\ incorporation = \frac{(\sum_{i=0}^{N} n_{M+i}\ * A)}{N}$$

193

194 Quantification of metabolites:
195 The relative quantification of total glucose, F1P, and GA3P levels were calculated
196 as the ratio derived from the sum of total ion counts of all isotopologues to their specific
197 internal standards (2DG for glucose and M6-F6P for F1P and GA3P respectively). The
198 absolute quantification of M+0 and M+6 fructose isotopologues were calculated as the
199 ratio of M+0 fructose ion counts or M+6 fructose ion counts to M+2 fructose ion counts
200 which is derived from the M2-fructose internal standard respectively.
201 For the quantification of glucose derived from any fructose carbons, we first
202 calculated the stable isotope enrichment of each isotopologue of glucose after correction
203 for the natural isotope distribution. Because fructose was administered as an equal
204 mixture of unlabeled and [U-^{13}C]-labeled fructose, levels of glucose derived from any
205 fructose carbons were calculated as twice the total glucose ion counts multiplied by the

206 corrected percentage of the sum of glucose isotopomers containing any ^{13}C. Levels of
207 glucose with three fructose-derived carbons were calculated as twice the total glucose
208 ion counts multiplied by the corrected percentage of M+3 glucose isotopomers.
209
210 Proteomics Sample Preparation:
211 Samples from mice treated with and without metformin (n=5) underwent large-
212 scale analysis of relative protein abundance changes as described previously [22]. For
213 each sample, approximately 15 mg of pulverized mouse intestinal tissue was solubilized
214 in ice-cold urea Lysis buffer (8 M urea in 50 mM Tris, pH 8.0, 40 mM NaCl, 2 mM $MgCl_2$,
215 1x Roche cOmplete ULTRA EDTA-free protease inhibitor mini tablet, 1x PhosStop
216 phosphatase inhibitor tablet, 5 mM NaF and 10 mM Na pyrophosphate). Samples were
217 lysed with a combination of disruption with a TissueLyzer (Qiagen) for 30 sec at 30 Hz,
218 subjected to three freeze-thaw cycles, and sonication with a probe sonicator. After
219 centrifugation at 10,000 g for 10 min at 4°C, protein concentration in the supernatant was
220 determined by BCA, and a 400 µg aliquot of each was adjusted to 2 mg/mL with Urea
221 Lysis Buffer. To reduce and alkylate cysteine residues, samples were incubated with 5
222 mM DTT at 32 °C for 30 min, cooled to RT, and incubated with 15 mM iodoacetamide for
223 30 min in the dark at RT. Following quenching of unreacted iodoacetamide by the addition
224 of equimolar DTT (up to 15 mM), samples were enzymatically digested with LysC (100:1
225 w/w, protein to enzyme) at 32 °C for 4 hr. After dilution to 1.5 M urea with 50 mM Tris (pH
226 8.0), 5 mM $CaCl_2$, samples were digested with trypsin (50:1 w/w, protein:enzyme)
227 overnight at 32 °C. Samples were acidified to 0.5% TFA and centrifuged at 10,000 ×g for
228 10 min at RT to pellet insoluble material. Supernatant containing soluble peptides was
229 subjected to solid phase extraction (SPE) with a Waters 50 mg tC18 SEP-PAK column to
230 remove salt, eluting once with 500 µL 25% acetonitrile/0.1% TFA and twice with 500 µL
231 50% acetonitrile/0.1% TFA. The eluate was frozen and dried by speed vac. Samples were
232 resuspended in 100 µL of 200 mM triethylammonium bicarbonate (TEAB), vortexed,
233 mixed with a different 10-plex Tandem Mass Tag (TMT) reagent (0.8 mg resuspended in
234 50 µL 100% acetonitrile), shaken for 4 hr at RT, and quenched with 0.8 µL 50%
235 hydroxylamine (shaking for 15 min at RT). All samples were mixed, frozen, and dried by
236 speed vac. The mixture was resuspended in 1 mL 0.5% TFA and subjected to SPE again

237 with a Waters 100 mg tC18 SEP-PAK SPE column as described above and the eluate
238 was frozen and dried by speed vac. The 4 mg TMT-labeled peptide mixture was
239 fractionated by high pH reversed-phase (HPRP) chromatography. After each of 12
240 fractions was lyophilized and resuspended in 1 mL 80% acetonitrile/0.15% TFA, 50 µL
241 was removed for analysis of unmodified peptides, frozen, and dried by speed vac.
242
243 Proteomics data acquisition:
244 Samples were analyzed by nanoflow liquid chromatography (nLC) on an EASY-nLC 1200
245 UH-PLC, followed by electrospray ionization (ESI) with an EASY-Spray source, and
246 tandem mass spectrometry (MS/MS) with a Q Exactive Plus Hybrid Quadrupole-Orbitrap
247 (Thermo Fisher Scientific). Sample fractions were resuspended in 22 µL of 0.1% FA and
248 were analyzed with triplicate runs, injecting 1 µL for the first and adjusting the volume for
249 subsequent runs to target an MS1 base peak intensity of 1×10^{10}. For each injection, the
250 sample was first trapped on an Acclaim PepMap 100 C18 trapping column (3 µg particle
251 size, 75 µm ×20 mm) with solvent A (0.1% FA) at a variable flow rate dictated by a
252 maximum pressure of 500 bar, after which the analytical separation was performed over
253 a 140 min gradient (flow rate of 300 nL/min) of 2% to 40% solvent B (90% ACN, 0.1%
254 FA) using an Acclaim Pep-Map RSLC C18 analytical column (2 µg particle size, 75µg
255 ×500 mm column (Thermo Fisher Scientific) with a column temperature of 55 °C. MS1
256 (precursor ions) was performed at 70,000 resolution with an AGC target of 3×10^{6} ions
257 and a maximum injection time (IT) of 60 ms. MS2 spectra (product ions) were collected
258 by data-dependent acquisition of the top 10 most abundant precursor ions with a charge
259 greater than 1 per MS1 scan, with dynamic exclusion enabled for a window of 30 s.
260 Precursor ions were filtered with a 0.7 m/z isolation window and fragmented with a
261 normalized collision energy of 30. MS2 scans were performed at 35,000 resolution, with
262 an AGC target of 1×10^{5} ions and a maximum IT of 60 ms.
263
264 Proteomics data analysis:
265 Raw files were processed with Proteome Discoverer 2.5 (PD2.5) from Thermo Fisher
266 Scientific. A complete mouse proteome fasta file containing 55,315 reviewed (Swiss-Prot)
267 and unreviewed (TrEMBL) protein sequences, downloaded from UniProt on 8/15/2022,

268 was imported into PD2.5. “Treatment” (metformin) versus “Water” (control) were
269 incorporated as “Study Factors”. MS1 precursor mass recalibration was performed after
270 a pre-search using the Spectrum Files RC node. Subsequent searches with Sequest HT
271 were conducted at 10 ppm (recalibrated) and 0.02 Da mass tolerances for precursor and
272 fragment ions, respectively. Modifications considered included oxidation on methionine
273 (variable + 15.995 Da), carbamidomethylation of cysteine (fixed + 57.021 Da), and
274 TMT6plex addition to lysine peptide N-termini (fixed + 229.163 Da). Searches allowed for
275 up to 2 missed K/R cleavages by trypsin (full specificity). Percolator [9] was used to filter
276 peptide spectral matches (PSMs) to an estimated FDR of less than 1%. The Peptide
277 Isoform Grouper node was used to collapse PSMs down to unique peptides, while
278 maintaining FDR < 1% at the peptide level. The Protein FDR Validator node was used to
279 group peptides into proteins using the rules of strict parsimony and maintain FDR < 1%
280 at the protein level. The Reporter Ion Quantifier node was used to filter PSMs for
281 quantitative quality, setting an upper threshold 50% precursor co-isolation and an average
282 reporter ion S/N> 2.5. For PSMs meeting these criteria, quantitative values were summed
283 together at the peptide and protein levels (after adjusting for TMT isotope impurities).
284 Unique peptides and Razor peptides were used for protein quantitation calculations,
285 excluding peptides with oxidized methionine. Quantitative values were normalized for any
286 deviations from equal total peptide signal on each TMT “channel”. Data were further
287 analyzed in R. PCA analysis was performed within each conditions, water and metformin
288 specifically, for outlier detection. One sample in each group appeared to be an extreme
289 outlier compared to the other samples in the group and were not used in subsequent
290 analysis. The remaining data were normalized before using DEseq2 for differential
291 analysis. Data visualization is conducted in R studio using ggplot2.
292
293 Western Blot:
294 20 to 30 mg intestinal tissue samples were homogenized in 0.5 mL cell signaling lysis
295 buffer that contains 20 mM Tris-HCl, 150 mM NaCl, 1 mM Na2EDTA, 1 mM EGTA, 1%
296 Triton and further supplemented with protease inhibitors (Sigma-Aldrich, P8340) and
297 phosphatase inhibitor cocktail (Pierce, A32957). After centrifugation at 12,000 g for 15
298 minutes, the supernatant was transferred to a fresh tube to measure protein concentration

299 using the BCA method (ThermoFisher, 23225). Approximately 35 ug of protein was
300 loaded per lane for SDS-PAGE electrophoresis. After electrophoresis, immunoproteins
301 were transferred to PVDF membranes. The membranes were then incubated with primary
302 antibodies overnight at 4 °C with gentle rocking after blocking with 5% solution of BSA
303 (Cytivia, SH30574.02) at room temperature for 1 hour. Primary antibodies used in this
304 work are as follows: anti-AMPK (Cell Signaling, 5831S), anti-AMPK (phospho T172)
305 antibody (Cell Signaling, 2635S), and anti-P85 (Upstate, 06-496). Blots were incubated
306 with appropriate secondary antibody after washing with TBST for 3 times.
307 Chemiluminescence was conducted using the Clarity Western ECL substrate kit (Bio-
308 Rad, 1705061) and membranes were imaged on ChemiDoc XP (Bio-Rad). Quantification
309 of blots was conducted using ChemiDoc XP associated Image Lab software v6.0. For
310 loading normalization, whole lane proteins were quantified using Bio-Rad Stain free
311 technology.
312
313 Statistics:
314 All data are presented as mean ± SEM. Comparison of metabolite levels between
315 the metformin group and controls were conducted using a two-tailed student's t-test in
316 GraphPad Prism. Statistical significance was assumed at p less than 0.05.
317
318 **Results**
319 **Short-term metformin treatment improves glucose tolerance without altering**
320 **fasting glycemia**
321 To investigate metformin's role in intestinal metabolism, 18-week-old wildtype
322 C57BL/6J mice were preconditioned with 1 week of high-fat, high-sucrose diet (45% Fat,
323 40% Sucrose) and then orally gavaged with metformin at a daily dose of 250 mg/kg of
324 body weight for two weeks. This dose of metformin in mice is reported to achieve
325 circulating concentrations of ~ 5 - 10 μM which is comparable to that in humans with Type-
326 2 Diabetes (T2D) taking 1 - 2 g metformin per day [23].
327 Metformin treatment did not affect body weight (Figure 1A, metformin: 33.5 ± 2.7
328 vs water: 34.2 ± 2.1 g). This is similar to observations that short-term metformin treatment
329 does not significantly impact body weight in human patients [24]. Fasting glycemia

330 remained similar between the metformin and control groups (Figure 1B). Whereas
331 metformin had no significant effect on body weight or fasting glycemia, 2 weeks of
332 metformin enhanced glucose tolerance (Figure 1C and D) with a reduction in glycemia at
333 the 30-minute time point (metformin: 292.44 ± 92.57 mg/dL vs water: 393.89 ± 87.23
334 mg/dL, $P<0.05$) and decreased area under the curve (metformin: 27790 ± 3326 A.U. vs
335 water: 34600 ± 2676 A.U., $P<0.05$). Thus, short-term metformin treatment enhanced
336 glucose tolerance without significant changes in body weight.
337

338 **Short-term metformin treatment decreases intestinal fructose metabolism and**
339 **fructose delivery to the liver**

340 The intestine is capable of robust fructose metabolism and a large portion of
341 intestinally metabolized fructose is used to produce glucose within intestinal tissue (Figure
342 2A) [17; 18]. After transport into the cell, fructose is first metabolized to fructose-1-
343 phosphate (F1P) followed by further metabolism to dihydroxyacetone phosphate (DHAP)
344 and glyceraldehyde (GA). Glyceraldehyde can be converted into glyceraldehyde-3-
345 phosphate (GA3P) via triokinase or into glycerate via aldehyde dehydrogenase. Glycerate
346 production tends to increase following a bolus of fructose and saturation of triokinase [25].
347 Fructose-derived triose phosphates then enter the glycolytic/gluconeogenic triose-
348 phosphate pool and can be used either for glucose production or can be further
349 metabolized to pyruvate/lactate and potentially enter the TCA cycle for oxidation. We
350 used ^{13}C-labeled fructose as a tracer to investigate the effects of metformin on intestinal
351 fructose and carbohydrate metabolism including glucose production. After a 5 hour fast,
352 we gavaged animals from both metformin and control groups with a 1:1 mixture of
353 unlabeled fructose and fructose that was universally labeled with carbon-13 ([U-^{13}C]-
354 fructose).

355 The levels of F1P were markedly reduced (from 14.20 ± 3.85 to 6.50 ± 3.54 A.U.,
356 $p<0.01$) in the intestinal tissue of animals treated with metformin versus water (Figure
357 2B). Metformin treatment reduced the enrichment of isotope-labeled three-carbon
358 metabolites, glyceraldehyde 3-phosphate (GA3P) and glycerate in intestinal tissue
359 (Figure 2C and D). These data indicate that fructose catabolism in intestinal tissue is
360 impaired by metformin treatment. Reductions in intestinal fructose metabolism could lead

361 to increased hepatic fructose delivery and contribute to fructose-induced metabolic
362 disease [26]. However, we observed that metformin treatment decreased portal vein M+0
363 and M+6 fructose levels by ~ 34% (Figure 2E). Reduced intestinal fructose metabolism
364 in combination with decreased portal fructose levels indicates that metformin impairs
365 intestinal fructose absorption. Additionally, the reduction in portal fructose following
366 metformin treatment indicates that metformin may reduce fructose delivery to the liver.
367 Consistent with this, metformin reduced levels of hepatic F1P (3.14 ± 1.59 to 1.25 ± 0.68
368 A.U., $p<0.05$, Figure 2F). Metformin treatment produced similar reductions in hepatic
369 GA3P levels (0.19 ± 0.10 to 0.08 ± 0.03 A.U., $p<0.05$, Figure 2G). Altogether, these results
370 indicate that two weeks of metformin treatment is sufficient to decrease intestinal fructose
371 metabolism and reduce fructose delivery to the liver.
372
373 **Short-term metformin treatment blunts intestinal glucose production**
374 At euthanasia - 30 minutes after fructose gavage - metformin reduced glucose
375 levels within intestinal tissue by 47% compared to control (Figure 3A). The reduced
376 glucose levels within intestinal tissue could be caused either by an increase in intestinal
377 glucose metabolism as suggested by experiments using FDG-glucose as a tracer [13],
378 reduced intestinal glucose production, or a combination of the two. Within intestinal tissue,
379 metformin also reduced the percentage of glucose containing fructose derived labeled
380 carbons (Figure 3B). At this time point, glycemia in systemic circulation is only reduced
381 by 13% in metformin treated mice compared to controls (Figure 3C). The labeling of
382 intestinal glucose with fructose-derived, labeled carbons is ~ 2-fold higher than in
383 peripheral circulation (Figure 3B and 3D). In combination, these results show that glucose
384 derived from fructose is being produced locally within the intestinal tissue. Glucose
385 produced from fructose within enterocytes is generated following metabolism of fructose
386 to trioses and will therefore predominately contain three fructose-derived carbons (Figure
387 2A and 3B). Within intestinal tissue, metformin reduced the labeling of glucose compared
388 to controls (Figure 3B) and reduced the levels of glucose containing any or three fructose-
389 derived carbons (Figure 3E and F) to a larger extent than glucose without fructose derived
390 carbons (Figure 3G). The reduction in intestinal glucose containing fructose-derived
391 carbons accounts for most of the reduction in intestinal glucose levels in the metformin

392 treated mice (comparing Fig 3A and 3E). Thus, the reduction in intestinal glucose
393 production from fructose is a major contributor to reduced intestinal glucose levels
394 following metformin treatment. This is consistent with metformin's effect to reduce
395 fructose absorption and metabolism as indicated in Figure 2.
396
397 **Short-term metformin treatment decreases fructose incorporation into the TCA**
398 **cycle.**
399 We previously demonstrated that fructose gavage rapidly labels the intestinal TCA
400 cycle pool which is a major contributor to circulating TCA cycle metabolites [27]. We next
401 investigated whether metformin also affects this process. The enrichment of labeled TCA
402 cycle intermediates was reduced in intestinal tissue of metformin treated mice (Figure 4A-
403 C). Metformin treatment produced a similar reduction in portal plasma TCA cycle
404 metabolite enrichment (Figure 4D-F). These data support our previous finding that the
405 intestine is a major source of circulating TCA cycle intermediates. Moreover, these results
406 indicate that labeling of circulating TCA cycle metabolites is responsive to metformin
407 treatment and measurement of this labeling pattern in blood may be a useful surrogate
408 index of intestinal metabolic function.
409 Whereas metformin uniformly reduced TCA cycle enrichment in both intestinal
410 tissue and portal blood samples, its effect on TCA cycle metabolite levels was mixed.
411 Metformin reduced citrate levels in both intestinal tissue and portal circulation (Figure 4G
412 and H). In contrast, metformin produced no changes in either tissue or circulating
413 succinate and produced an isolated increase in portal malate levels without a change in
414 malate in intestinal tissue although the variance was high for malate measurements in
415 tissue. The changes in TCA cycle metabolite levels may suggest that metformin inhibits
416 malate to citrate conversion in the TCA cycle, potentially via inhibition of malate
417 dehydrogenase. This would be consistent with metformin's purported effects to inhibit
418 Complex I activity as malate dehydrogenase donates electrons to Complex I and its
419 activity is closely coupled to that of the electron transport chain [28-31].
420

421 **Metformin reduces the abundance of intestinal proteins involved in carbohydrate**
422 **metabolism.**

423 As isotope-tracing metabolomics indicated that metformin reduced intestinal
424 fructose catabolism and glucose production, we next aimed to investigate molecular
425 mechanisms contributing to these changes via proteomics in intestinal tissue. In total,
426 5328 proteins were quantified and annotated via our discovery proteomics
427 (Supplementary Table 2). Principal component analysis (PCA) using all quantified
428 proteins identified two clusters that separate the treatment groups (Figure 5A). However,
429 the 95% confidence intervals for the metformin and control clusters overlap suggesting
430 that global protein expression levels within the intestine were not markedly different
431 between treatment conditions (Figure 5A).

432 A total of 1942 proteins were identified as differentially abundant between
433 metformin and control groups using a p-value less than 0.05 (two-tailed student's t-test).
434 After adjusting for repeated measures by the Benjamini and Hochberg method, a total of
435 219 proteins were identified as differentially abundant with an adjusted P-value less than
436 0.05 and an absolute $\log_2$ fold-change greater than 0.5 (Figure 5B and Supplementary
437 Table 3). Many of the top-ranked differentially abundant proteins are associated with
438 metabolic process including gluconeogenic enzymes such as Fbp1 and G6pc (Figure 5B).
439 Despite variability in protein abundance levels within groups, unsupervised K-means
440 clustering segregated metformin treated from untreated mice (Figure 5C). Pathway
441 analysis using differentially expressed proteins with an adjusted P-value less than 0.05
442 suggested that metformin treatment affected multiple metabolic pathways in the intestinal
443 tissue (Supplementary Table 4 and 5). One of the top down-regulated pathways in
444 intestinal tissue from the metformin group is "Glycolysis and Gluconeogenesis (WP157)"
445 (Figure 5D). Other metabolic pathways demonstrating downregulation with metformin
446 treatment include the "Electron Transport Chain (WP295)" and "Oxidative
447 Phosphorylation", pathways potentially complementary to the putative effects of
448 metformin to inhibit mitochondrial function [32; 33] (Figure 5D). In addition, proteins
449 associated with both glycolysis and gluconeogenic pathways, including pyruvate
450 carboxykinase (Pck1), Fructose 1,6-bisphosphatase (Fbp1), glucose 6-phosphatase
451 (G6pc1), lactate dehydrogenase (Ldhb), pyruvate dehydrogenase (Pdh1), malate

452 dehydrogenase (Mdh2), enolase 1 (Eno1), hexokinase (Hk1), pyruvate kinase (Pkm),
453 bisphosphoglycerate mutase (Bpgm), were markedly down-regulated in the metformin
454 group compared to controls (Figure 5E). Similarly, hexose transporters capable of
455 fructose transport including both GLUT5 (Slc2a5) and GLUT2 (Slc2a2), as well as key
456 fructolytic enzymes ketohexokinase (Khk) and aldolase, fructose-bisphosphate B (Aldob)
457 were all significantly down-regulated in metformin treated intestinal tissues (Figure 5F).
458 The reduction in glycolytic, gluconeogenic, and fructolytic transporters and enzymes are
459 consistent with the results from the metabolomic tracer studies that indicate that
460 metformin impairs intestinal fructose absorption and catabolism as well as glucose
461 production.
462

463 **Activation of AMPK signaling is likely to impact metformin's effects on intestinal**
464 **metabolic functions**

465 The proteomics study suggests that mitochondria, and especially the electron
466 transport chain, are impacted by metformin treatment through coordinate downregulation
467 of many of its constituent proteins (Figure 5D, Figure 6A, and Supplementary Table 4).
468 The ability of metformin to impact mitochondrial function is well documented [32-35].
469 Activation of AMPK is purported to play a central role in metformin's mechanism of action
470 and activation of AMPK may be mediated via metformin's ability to inhibit mitochondrial
471 Complex I and via other mechanisms [32; 36; 37]. We examined the abundance levels of
472 detectable proteins quantified in our proteomics data that are annotated within the "AMPK
473 signaling pathway (KEGG: mmu04152)" and conducted a PCA analysis using these 50
474 proteins. As is indicated in Figure 6B, expression of components of the AMPK signaling
475 pathway in the intestine samples from metformin versus control treated mice tend to
476 segregate based on the first and second principal components (PC1 and PC2,
477 Supplementary Table 5). Our intestinal proteomics study only detected the α (Prkaa1,
478 Prkaa2) and γ subunits (Prkag1) of AMPK component (Figure 6C). Among these, the
479 abundance of Prkaa1 significantly decreased after metformin treatment while Prkaa2
480 tended to increase (Figure 6C). To further examine the role of AMPK signaling, we
481 measured the total protein levels of AMPKα and the phosphorylation of AMPKα at the Thr
482 172 site, a marker of AMPK activation. As expected, metformin treatment increased the

483 phosphorylation level of AMPKα Thr172 indicating that short-term metformin treatment
484 activates intestinal AMPK signaling (Figure 6D and E).
485
486 **Discussion**
487 Metformin is a widely prescribed anti-diabetic drug with uncertain target tissues
488 and mechanism of action. Identification of metformin's target tissue will facilitate the
489 understanding of metformin's glucose lowering effects and may promote the development
490 of additional therapies for metabolic diseases. Previous studies suggested the potential
491 of the intestine as an important metformin target since metformin concentrates to high
492 levels in intestinal tissue [11; 12]. Intravenous administration of metformin or reducing
493 intestinal metformin absorption impairs metformin's effects to lower glucose production
494 [38; 39]. Few studies have investigated the role of metformin on intestinal function and its
495 association with systemic glucose homeostasis. Among the studies focusing on the
496 intestine, the beneficial effects of metformin were suggested to closely associated with its
497 role on stimulating intestinal secretion of GLP-1 and GDF15 which are known to regulate
498 systemic glucose homeostasis [23; 33; 40]. To our knowledge, no study has directly
499 assessed metformin's effects on intestinal metabolic function using stable isotopic
500 tracers. In this study, we assessed intestinal fructose metabolism after an oral fructose
501 bolus (1:1 ratio of unlabeled:^{13}C-labeled fructose) to probe intestinal carbohydrate
502 metabolism after short-term metformin treatment. This methodology is based on recent
503 findings from our lab and others that fructose is rapidly metabolized in the small intestine
504 and can be readily used by the intestine to produce glucose [17; 18].
505 In this study, we observed that 30 minutes after fructose gavage, the majority of
506 glucose within intestinal tissue contained fructose-derived carbons and half contained
507 three fructose-derived carbons (Figure 3A, E, and F) in both metformin treated mice and
508 controls. In systemic circulation, enrichment of glucose with fructose-derived carbon was
509 ~ 50% lower than in intestinal tissue (Figure 3B vs 3D) indicative of dilution of intestinally
510 derived glucose in systemic circulation. This supports prior work indicating that fructose
511 is readily used as metabolic substrate for glucose production in the intestine and this
512 contributes significantly to whole-body glucose production [17; 18]. Our data

513 demonstrates that short-term metformin treatment reduced intestinal glucose production
514 from fructose and fructose delivery to the liver (Figure 2 and 3).
515 Metformin reduced intestinal glucose production, and this is associated with
516 enhanced glucose tolerance (Figure 1C and D). Importantly, these beneficial effects
517 occurred prior to significant weight changes (Figure 1A). Whether the effect of metformin
518 to reduce intestinal glucose production is a major mechanism by which metformin
519 enhances systemic glucose tolerance remains to be defined.
520 With the prevalence of high fructose corn syrup in the typical Western diet, the
521 potential for fructose consumption as a contributor to metabolic disease has attracted
522 increasing attention [41]. Studies conducted in both human and rodents support the
523 hypothesis that excessive fructose consumption can contribute to metabolic disorders
524 including obesity, insulin resistance, and NAFLD [42-44]. Intestinal tissue is a major site
525 of fructose metabolism and shields the liver from fructose induced metabolic disease [17],
526 as hepatic fructose metabolism is essential for the development of fructose related
527 pathologies like increased de novo lipogenesis, steatosis, and insulin resistance [26]. A
528 prior study suggested that fructose-induced metabolic disease may be attenuated by
529 metformin treatment in mice although this was attributed to an effect of metformin to alter
530 the microbiome and protect against deterioration of gut barrier function [45]. Our results
531 are consistent with a protective effect of metformin against fructose-induced metabolic
532 disease as we demonstrated that metformin decreased fructose delivery to the liver
533 (Figure 2E-G). These results might point towards a particularly beneficial effect of
534 metformin in people with diabetes and metabolic disease that consume excessive
535 amounts of dietary sugar.
536 In addition to decreasing fructose delivery to the liver, we also demonstrated that
537 metformin decreased intestinal fructose metabolism. Specifically, intestinal F1P levels
538 were nearly halved in the intestinal tissue of metformin treated animals when compared
539 to controls (Figure 2B). Additionally, significantly lower enrichment of isotope labeling was
540 detected in the downstream three-carbon phosphates and TCA cycle metabolites (Figure
541 2C and D, Figure 4 A-C). It is interesting that metformin treatment not only decreased
542 intestinal fructose metabolism, but also reduced the amount of fructose delivered to the
543 liver, suggesting the possibility that metformin treatment reduced intestinal fructose

544 absorption. Indeed, unbiased proteomics indicated that the abundance of luminal fructose
545 transporter GLUT5 and the basolateral glucose/fructose transporter GLUT2 were both
546 reduced by metformin treatment (Figure 5F). This finding seems contradictory to a recent
547 study where metformin increased GLUT2 expression in the colon and to a lesser extent
548 in the ileum [13]. This discrepancy may be due in part to differences in intestinal segments
549 analyzed between the two studies. Further investigation will be required to determine the
550 impact of metformin on distinct intestinal segments.

551 Gastrointestinal symptoms including bloating and diarrhea are the most prevalent
552 side effects of metformin treatment and these symptoms are often experienced in the first
553 few weeks following treatment initiation [46]. It is also well-established that defects in
554 intestinal fructose metabolism can cause significant GI disturbances [47-50]. It is
555 interesting to speculate that the ability of metformin to impair fructose absorption may
556 contribute to its unwanted gastrointestinal effects. Future studies may include
557 investigation into how metformin alters intestinal epithelial absorptive function and
558 substrate transport.

559 Most studies investigating metformin's mechanism of action focus on specific
560 putative targets include Complex 1, AMPK, mitochondrial glycerophosphate
561 dehydrogenase, PEN2, and others [14; 36; 45; 51; 52]. Unexpectedly, our proteomics
562 data conducted on metformin treated intestinal tissue suggests that metformin produces
563 broad-based reductions in the levels of many metabolic enzymes including key enzymes
564 in glycolytic, gluconeogenic, and fructolytic pathways. These results are consistent with
565 our conclusions regarding metformin's multiple metabolic effects derived from isotope
566 tracing data that fructose metabolism, glucose production, and other aspects of intestinal
567 carbohydrate metabolism are all significantly impacted by metformin treatment. This novel
568 finding extends our knowledge of metformin's potential mechanistic effects and points to
569 novel mechanisms of action.

570 Broad-based effects of metformin on the levels of components of the mitochondrial
571 electron transport chain are also indicated by the proteomics data analysis. Metformin is
572 known to regulate mitochondrial function by inhibiting Complex I of the mitochondrial
573 electron transport chain [36]. However, the physiological relevance of this mechanism is
574 debated as this mechanism requires high concentrations of metformin (~ 150 μM) within

575 the mitochondrial matrix [28]. At the therapeutically relevant doses that we used in this
576 study, we observed that metformin reduced citrate levels and increased malate levels in
577 the portal circulation (Figure 4G and H). This suggests inhibition of malate dehydrogenase
578 and Complex I of the electron transport chain as malate dehydrogenase activity is coupled
579 to Complex I activity. However, as the proteomics analysis indicated that the expression
580 levels of many Complex I subunits including multiple Ndufa, Ndufb and Ndufs subunits
581 were significantly down-regulated by metformin treatment (Figure 6A), we cannot
582 determine whether metformin's apparent effect to inhibit Complex I activity might be
583 mediated by direct inhibition or through metformin's more general effect to reduce levels
584 of Complex I components.

585 AMPK activation is often invoked as a key mechanism mediating metformin action
586 [7; 32]. Although, recent studies suggest metformin relies on both AMPK-dependent and
587 AMPK-independent mechanisms to mediate its beneficial effects [9]. We also observed
588 that the intestinal AMPK signaling was impacted by metformin treatment (Figure 6C and
589 D). Metformin increased phosphorylation of AMPK at Thr172 potentially consistent with
590 increased AMP/ATP ratio (Figure 6E and F). Again, because of the broad-based effects
591 of metformin on metabolic and mitochondrial protein levels, we cannot readily define the
592 mechanism by which metformin treatment leads to AMPK activation. Neither could we
593 determine whether AMPK signaling participates in metformin's effects to reduce intestinal
594 fructose metabolism and glucose production.

595 This study supports our recent work indicating that the intestine is a major source
596 of circulating TCA cycle intermediates [27], and that measurement of fructose-derived
597 label in portal and possibly peripheral circulating blood TCA cycle metabolites may
598 provide a useful index of intestinal metabolic function. In the future this approach may be
599 useful for assessing intestinal metabolic function in large-scale human studies and has
600 the potential to open new avenues for investigating intestinal metabolic function in a wide
601 range of scenarios. In this study, we used this approach to demonstrate that the intestine
602 is a target for therapeutic doses of metformin and short-term metformin treatment impacts
603 intestinal glucose and fructose metabolism. Moreover, proteomics analysis suggests that
604 metformin reduces the intestinal levels of a broad array of metabolic enzymes and
605 transporters involved in sugar metabolism. Additional work will be required to define

606 mechanisms by which metformin reduces the levels metabolic enzymes and impacts key
607 metabolic pathways within the intestine to enhance glucose homeostasis.
608
609
610 **Author Contributions:**
611 **MAH, WT, SAH, AS and IA** designed, performed, and interpreted the mouse
612 experiments. **GZ, WT, MAH, and SAH** designed, performed, and interpreted
613 metabolomics analysis. **PAG, MAH, IA, and WT** designed, performed, and interpreted
614 proteomics analysis. **MAH** conceived of, designed, and supervised the experimental plan,
615 and interpreted experiments. **WT** and **MAH** wrote the manuscript. All authors edited the
616 manuscript.
617
618 **Acknowledgements:**
619 This work was supported by NIH grant 5R01 DK121710 (MAH). Metabolomics support
620 was provided by the North Carolina Diabetes Research Center (NCDRC) (P30
621 DK124723).
622
623 **Figure Legends:**
624 **Figure 1. Short-term metformin treatment improves glucose tolerance without**
625 **reducing body weight and fasting glycemia levels.**
626 (A) Body weight before and after metformin versus water treatment. (B) Fasting
627 glycemia levels after 2 weeks of treatment. (C - D) Intraperitoneal glucose tolerance test
628 after 2 weeks of treatment. Data represent means ± SEM. n=9 per group * $p<0.05$; **
629 $p<0.01$; *** $p<0.001$. Analysis performed via paired student-t test.
630
631 **Figure 2. Short-term metformin treatment is sufficient to decrease fructose**
632 **catabolism in the intestinal tissue and fructose delivery to the liver.**
633 (A) Diagram showing the fructose catabolism pathways within enterocytes. (B)
634 Relative quantity of fructose 1-phosphate, and enrichment of (C) glyceraldehyde 3-
635 phosphate, and (D) glycerate in the intestinal tissue 30 minutes after fructose gavage in
636 mice treated with water versus metformin for 2 weeks. (E) Absolute fructose levels

637 measured in the portal blood. (F) Relative quantification of fructose 1-phosphate and (G)
638 glyceraldehyde 3-phosphate in the liver tissue after fructose gavage. 0.1 nmol M6-
639 Fructose 6-phosphate and 4 nmol M2-fructose were used as internal standard for the
640 measurement of fructose 1-phosphate and fructose respectively. Norvaline was used as
641 the internal standard for the measurement of glyceraldehyde 3-phosphate, and glycerate.
642 Data represent means ± SEM. * $p<0.05$; ** $p<0.01$; *** $p<0.001$. Analysis performed via
643 paired student-t test.
644
645 **Figure 3. Short-term metformin treatment reduces glucose production from**
646 **fructose in intestinal tissue.**
647 (A) Relative glucose levels and (B) the enrichment of glucose with labeled fructose tracer
648 in intestinal tissue. (C) Relative circulating glucose and (D) enrichment of glucose
649 measured in tail vein plasma. The levels of glucose with (E) any, (F) three, and (G) no
650 carbons derived from fructose in intestinal tissue. 2 nmol 2-Deoxu-D-glucose (2DG) was
651 used as internal standard for the measurement of glucose. Data represent means ± SEM.
652 * $p<0.05$; ** $p<0.01$; *** $p<0.001$. Analysis performed via paired student-t test.
653
654 **Figure 4. Short-term metformin treatment reduces production of intestinal TCA**
655 **cycle intermediates from fructose.**
656 The enrichment of (A) succinate, (B) malate, and (C) citrate in intestinal tissue 30 minutes
657 after fructose gavage in mice treated with water versus metformin for 2 weeks. The
658 enrichment of (D) succinate, (E) malate, and (F) citrate in the portal plasma after fructose
659 gavage. Relative quantification of TCA cycle metabolites in the (G) intestinal tissue, and
660 (H) portal circulation. Norvaline was used as the internal standard for these
661 measurements. Data represent means ± SEM. * $p<0.05$; ** $p<0.01$; *** $p<0.001$. Analysis
662 performed via paired student-t test.
663
664 **Figure 5. Proteomics demonstrates down-regulation of proteins involved in**
665 **carbohydrate metabolism in intestinal tissue.**
666 (A) Principal component analysis of quantitative proteomics data generated from the
667 intestinal tissue samples of mice treated with water versus metformin. (B) Volcano plot

668 and (C) K-means clustering heatmap of differentially abundant proteins in the intestinal
669 tissue samples from water versus metformin groups. (D) Pathway analysis using proteins
670 that are significantly down-regulated in the intestinal tissue samples of metformin versus
671 water group. (E) Significantly altered protein levels in the gluconeogenesis pathway as
672 well as key hexose transporters and fructolytic enzymes. Analysis performed in R using
673 data generated from Proteome Discoverer.
674
675 **Figure 6. Short-term metformin treatment impacts mitochondrial components and**
676 **activates AMPK signaling.**
677 (A) Metformin reduces protein levels of components of the electron transport chain in
678 intestinal tissue. (B) Principal component analysis using proteins annotated in the AMPK
679 signaling pathway (KEGG: mmu04152). (C-D) Intestinal protein abundance in AMPK
680 signaling pathway in water versus metformin group. (E-F) Western blot and quantification
681 of the expression levels of AMPKα and phospho-AMPKα T172. Analysis within panel A
682 and B was performed with R using data generated from Proteome Discoverer. Data in
683 panel F represent as means ± SEM and paired student-t test was used for statistical
684 analysis. * $p<0.05$; ** $p<0.01$; *** $p<0.001$.
685

Reference

[1] Sanchez-Rangel, E., Inzucchi, S.E., 2017. Metformin: clinical use in type 2 diabetes. Diabetologia 60(9):1586-1593.

[2] Yerevanian, A., Soukas, A.A., 2019. Metformin: Mechanisms in Human Obesity and Weight Loss. Curr Obes Rep 8(2):156-164.

[3] Lin, H.Z., Yang, S.Q., Chuckaree, C., Kuhajda, F., Ronnet, G., Diehl, A.M., 2000. Metformin reverses fatty liver disease in obese, leptin-deficient mice. Nat Med 6(9):998-1003.

[4] Farr, S.A., Roesler, E., Niehoff, M.L., Roby, D.A., McKee, A., Morley, J.E., 2019. Metformin Improves Learning and Memory in the SAMP8 Mouse Model of Alzheimer's Disease. J Alzheimers Dis 68(4):1699-1710.

[5] Cerezo, M., Tichet, M., Abbe, P., Ohanna, M., Lehraiki, A., Rouaud, F., et al., 2013. Metformin blocks melanoma invasion and metastasis development in AMPK/p53-dependent manner. Mol Cancer Ther 12(8):1605-1615.

[6] Linnard-Palmer, L., 2012. The use of simulation for pediatric oncology nursing safety principles: ensuring competent practice through the use of a mnemonic, chemotherapy road maps and case-based learning. J Pediatr Nurs 27(3):283-286.

[7] Hundal, R.S., Krssak, M., Dufour, S., Laurent, D., Lebon, V., Chandramouli, V., et al., 2000. Mechanism by which metformin reduces glucose production in type 2 diabetes. Diabetes 49(12):2063-2069.

[8] LaMoia, T.E., Shulman, G.I., 2021. Cellular and Molecular Mechanisms of Metformin Action. Endocr Rev 42(1):77-96.

[9] Rena, G., Hardie, D.G., Pearson, E.R., 2017. The mechanisms of action of metformin. Diabetologia 60(9):1577-1585.

[10] Foretz, M., Guigas, B., Bertrand, L., Pollak, M., Viollet, B., 2014. Metformin: from mechanisms of action to therapies. Cell Metab 20(6):953-966.

[11] Tanja, J.J., Langlass, T.M., 1995. Metformin: a biguanide. Diabetes Educ 21(6):509-510, 513-504.

[12] Zhang, Q., Hu, N., 2020. Effects of Metformin on the Gut Microbiota in Obesity and Type 2 Diabetes Mellitus. Diabetes Metab Syndr Obes 13:5003-5014.

[13] Tobar, N., Rocha, G.Z., Santos, A., Guadagnini, D., Assalin, H.B., Camargo, J.A., et al., 2023. Metformin acts in the gut and induces gut-liver crosstalk. Proc Natl Acad Sci U S A 120(4):e2211933120.

[14] Ma, T., Tian, X., Zhang, B., Li, M., Wang, Y., Yang, C., et al., 2022. Low-dose metformin targets the lysosomal AMPK pathway through PEN2. Nature 603(7899):159-165.

[15] Yılmaz, S., Ozhan, M., Sager, S., Yörük Atik, D., Halac, M., Sönmezoğlu, K., 2011. Metformin-Induced Intense Bowel Uptake Observed on Restaging FDG PET/CT Study in a Patient with Gastric Lymphoma. Mol Imaging Radionucl Ther 20(3):114-116.

[16] Massollo, M., Marini, C., Brignone, M., Emionite, L., Salani, B., Riondato, M., et al., 2013. Metformin temporal and localized effects on gut glucose metabolism assessed using 18F-FDG PET in mice. J Nucl Med 54(2):259-266.

[17] Jang, C., Hui, S., Lu, W., Cowan, A.J., Morscher, R.J., Lee, G., et al., 2018. The Small Intestine Converts Dietary Fructose into Glucose and Organic Acids. Cell Metab 27(2):351-361.e353.

729 [18] Bismut, H., Hers, H.G., Van Schaftingen, E., 1993. Conversion of fructose to glucose in
730 the rabbit small intestine. A reappraisal of the direct pathway. Eur J Biochem 213(2):721-726.
731 [19] Bu, P., Chen, K.Y., Xiang, K., Johnson, C., Crown, S.B., Rakhilin, N., et al., 2018. Aldolase
732 B-Mediated Fructose Metabolism Drives Metabolic Reprogramming of Colon Cancer Liver
733 Metastasis. Cell Metab 27(6):1249-1262.e1244.
734 [20] Fernandez, C.A., Des Rosiers, C., Previs, S.F., David, F., Brunengraber, H., 1996.
735 Correction of 13C mass isotopomer distributions for natural stable isotope abundance. J Mass
736 Spectrom 31(3):255-262.
737 [21] Zhang, G.F., Jensen, M.V., Gray, S.M., El, K., Wang, Y., Lu, D., et al., 2020. Reductive
738 TCA cycle metabolism fuels glutamine- and glucose-stimulated insulin secretion. Cell Metab.
739 [22] Lyons, S.P., Wilson, R.J., Muoio, D.M., Grimsrud, P.A., 2022. Proteomics and
740 phosphoproteomics datasets of a muscle-specific STIM1 loss-of-function mouse model. Data
741 Brief 42:108051.
742 [23] Coll, A.P., Chen, M., Taskar, P., Rimmington, D., Patel, S., Tadross, J.A., et al., 2020.
743 GDF15 mediates the effects of metformin on body weight and energy balance. Nature
744 578(7795):444-448.
745 [24] Jensterle Sever, M., Kocjan, T., Pfeifer, M., Kravos, N.A., Janez, A., 2014. Short-term
746 combined treatment with liraglutide and metformin leads to significant weight loss in obese
747 women with polycystic ovary syndrome and previous poor response to metformin. Eur J
748 Endocrinol 170(3):451-459.
749 [25] Liu, L., Li, T., Liao, Y., Wang, Y., Gao, Y., Hu, H., et al., 2020. Triose Kinase Controls the
750 Lipogenic Potential of Fructose and Dietary Tolerance. Cell Metab 32(4):605-618.e607.
751 [26] Andres-Hernando, A., Orlicky, D.J., Kuwabara, M., Ishimoto, T., Nakagawa, T., Johnson,
752 R.J., et al., 2020. Deletion of Fructokinase in the Liver or in the Intestine Reveals Differential
753 Effects on Sugar-Induced Metabolic Dysfunction. Cell Metab 32(1):117-127.e113.
754 [27] Tong, W., Hannou, S.A., Wang, Y., Astapova, I., Sargsyan, A., Monn, R., et al., 2022. The
755 intestine is a major contributor to circulating succinate in mice. Faseb j 36(10):e22546.
756 [28] Owen, M.R., Doran, E., Halestrap, A.P., 2000. Evidence that metformin exerts its anti-
757 diabetic effects through inhibition of complex 1 of the mitochondrial respiratory chain. Biochem
758 J 348 Pt 3(Pt 3):607-614.
759 [29] Lee, P., Leong, W., Tan, T., Lim, M., Han, W., Radda, G.K., 2013. In vivo hyperpolarized
760 carbon-13 magnetic resonance spectroscopy reveals increased pyruvate carboxylase flux in an
761 insulin-resistant mouse model. Hepatology 57(2):515-524.
762 [30] Wang, Q., Yu, L., Yu, C.A., 2010. Cross-talk between mitochondrial malate
763 dehydrogenase and the cytochrome bc1 complex. J Biol Chem 285(14):10408-10414.
764 [31] Ovádi, J., Huang, Y., Spivey, H.O., 1994. Binding of malate dehydrogenase and NADH
765 channelling to complex I. J Mol Recognit 7(4):265-272.
766 [32] Wang, Y., An, H., Liu, T., Qin, C., Sesaki, H., Guo, S., et al., 2019. Metformin Improves
767 Mitochondrial Respiratory Activity through Activation of AMPK. Cell Rep 29(6):1511-
768 1523.e1515.
769 [33] Yang, M., Darwish, T., Larraufie, P., Rimmington, D., Cimino, I., Goldspink, D.A., et al.,
770 2021. Inhibition of mitochondrial function by metformin increases glucose uptake, glycolysis
771 and GDF-15 release from intestinal cells. Sci Rep 11(1):2529.

772 [34] Vial, G., Detaille, D., Guigas, B., 2019. Role of Mitochondria in the Mechanism(s) of
773 Action of Metformin. Front Endocrinol (Lausanne) 10:294.
774 [35] Soberanes, S., Misharin, A.V., Jairaman, A., Morales-Nebreda, L., McQuattie-Pimentel,
775 A.C., Cho, T., et al., 2019. Metformin Targets Mitochondrial Electron Transport to Reduce Air-
776 Pollution-Induced Thrombosis. Cell Metab 29(2):335-347.e335.
777 [36] Wheaton, W.W., Weinberg, S.E., Hamanaka, R.B., Soberanes, S., Sullivan, L.B., Anso, E.,
778 et al., 2014. Metformin inhibits mitochondrial complex I of cancer cells to reduce tumorigenesis.
779 Elife 3:e02242.
780 [37] Ling, S., Shan, Q., Liu, P., Feng, T., Zhang, X., Xiang, P., et al., 2017. Metformin
781 ameliorates arsenic trioxide hepatotoxicity via inhibiting mitochondrial complex I. Cell Death
782 Dis 8(11):e3159.
783 [38] Buse, J.B., DeFronzo, R.A., Rosenstock, J., Kim, T., Burns, C., Skare, S., et al., 2016. The
784 Primary Glucose-Lowering Effect of Metformin Resides in the Gut, Not the Circulation: Results
785 From Short-term Pharmacokinetic and 12-Week Dose-Ranging Studies. Diabetes Care 39(2):198-
786 205.
787 [39] Sum, C.F., Webster, J.M., Johnson, A.B., Catalano, C., Cooper, B.G., Taylor, R., 1992. The
788 effect of intravenous metformin on glucose metabolism during hyperglycaemia in type 2
789 diabetes. Diabet Med 9(1):61-65.
790 [40] Gontier, E., Fourme, E., Wartski, M., Blondet, C., Bonardel, G., Le Stanc, E., et al., 2008.
791 High and typical 18F-FDG bowel uptake in patients treated with metformin. Eur J Nucl Med
792 Mol Imaging 35(1):95-99.
793 [41] Herman, M.A., Birnbaum, M.J., 2021. Molecular aspects of fructose metabolism and
794 metabolic disease. Cell Metab 33(12):2329-2354.
795 [42] Khan, T.A., Sievenpiper, J.L., 2016. Controversies about sugars: results from systematic
796 reviews and meta-analyses on obesity, cardiometabolic disease and diabetes. Eur J Nutr
797 55(Suppl 2):25-43.
798 [43] Ma, J., McKeown, N.M., Hwang, S.J., Hoffmann, U., Jacques, P.F., Fox, C.S., 2016. Sugar-
799 Sweetened Beverage Consumption Is Associated With Change of Visceral Adipose Tissue Over
800 6 Years of Follow-Up. Circulation 133(4):370-377.
801 [44] Toop, C.R., Gentili, S., 2016. Fructose Beverage Consumption Induces a Metabolic
802 Syndrome Phenotype in the Rat: A Systematic Review and Meta-Analysis. Nutrients 8(9).
803 [45] Spruss, A., Kanuri, G., Stahl, C., Bischoff, S.C., Bergheim, I., 2012. Metformin protects
804 against the development of fructose-induced steatosis in mice: role of the intestinal barrier
805 function. Lab Invest 92(7):1020-1032.
806 [46] Subramaniam, K., Joseph, M.P., Babu, L.A., 2021. A Common Drug Causing a Common
807 Side Effect at an Uncommon Time: Metformin-Induced Chronic Diarrhea and Weight Loss
808 After Years of Treatment. Clin Diabetes 39(2):237-240.
809 [47] Choi, Y.K., Johlin, F.C., Jr., Summers, R.W., Jackson, M., Rao, S.S., 2003. Fructose
810 intolerance: an under-recognized problem. Am J Gastroenterol 98(6):1348-1353.
811 [48] Barone, S., Fussell, S.L., Singh, A.K., Lucas, F., Xu, J., Kim, C., et al., 2009. Slc2a5 (Glut5)
812 is essential for the absorption of fructose in the intestine and generation of fructose-induced
813 hypertension. J Biol Chem 284(8):5056-5066.

814 [49] Patel, C., Douard, V., Yu, S., Gao, N., Ferraris, R.P., 2015. Transport, metabolism, and
815 endosomal trafficking-dependent regulation of intestinal fructose absorption. Faseb j 29(9):4046-
816 4058.
817 [50] Kim, M., Astapova, II, Flier, S.N., Hannou, S.A., Doridot, L., Sargsyan, A., et al., 2017.
818 Intestinal, but not hepatic, ChREBP is required for fructose tolerance. JCI Insight 2(24).
819 [51] Cao, J., Meng, S., Chang, E., Beckwith-Fickas, K., Xiong, L., Cole, R.N., et al., 2014. Low
820 concentrations of metformin suppress glucose production in hepatocytes through AMP-
821 activated protein kinase (AMPK). J Biol Chem 289(30):20435-20446.
822 [52] Thakur, S., Daley, B., Gaskins, K., Vasko, V.V., Boufraqech, M., Patel, D., et al., 2018.
823 Metformin Targets Mitochondrial Glycerophosphate Dehydrogenase to Control Rate of
824 Oxidative Phosphorylation and Growth of Thyroid Cancer In Vitro and In Vivo. Clin Cancer
825 Res 24(16):4030-4043.
826

Figure1

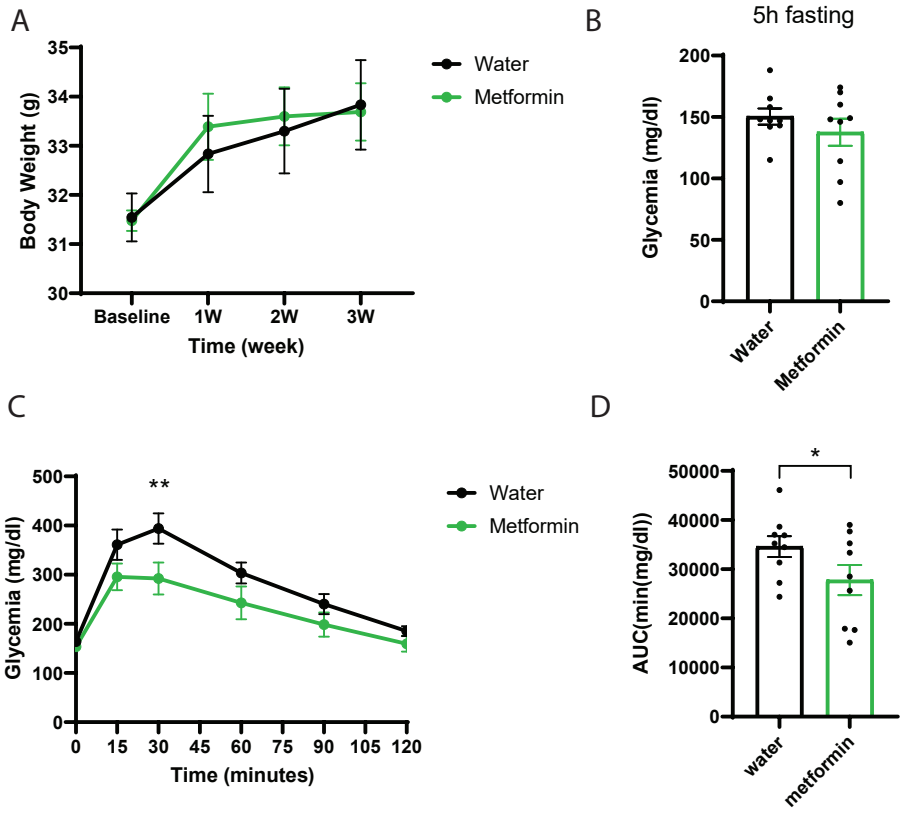
A
Body Weight (g)
35
34
33
32
31
30
Baseline
1W
2W
3W
Time (week)
Water
Metformin
B
5h fasting
Glycemia (mg/dl)
200
150
100
50
0
Water
Metformin
C
Glycemia (mg/dl)
500
400
300
200
100
0
**
0
15
30
45
60
75
90
105
120
Time (minutes)
Water
Metformin
D
AUC(min(mg/dl))
50000
40000
30000
20000
10000
0
*
water
metformin

Figure 2

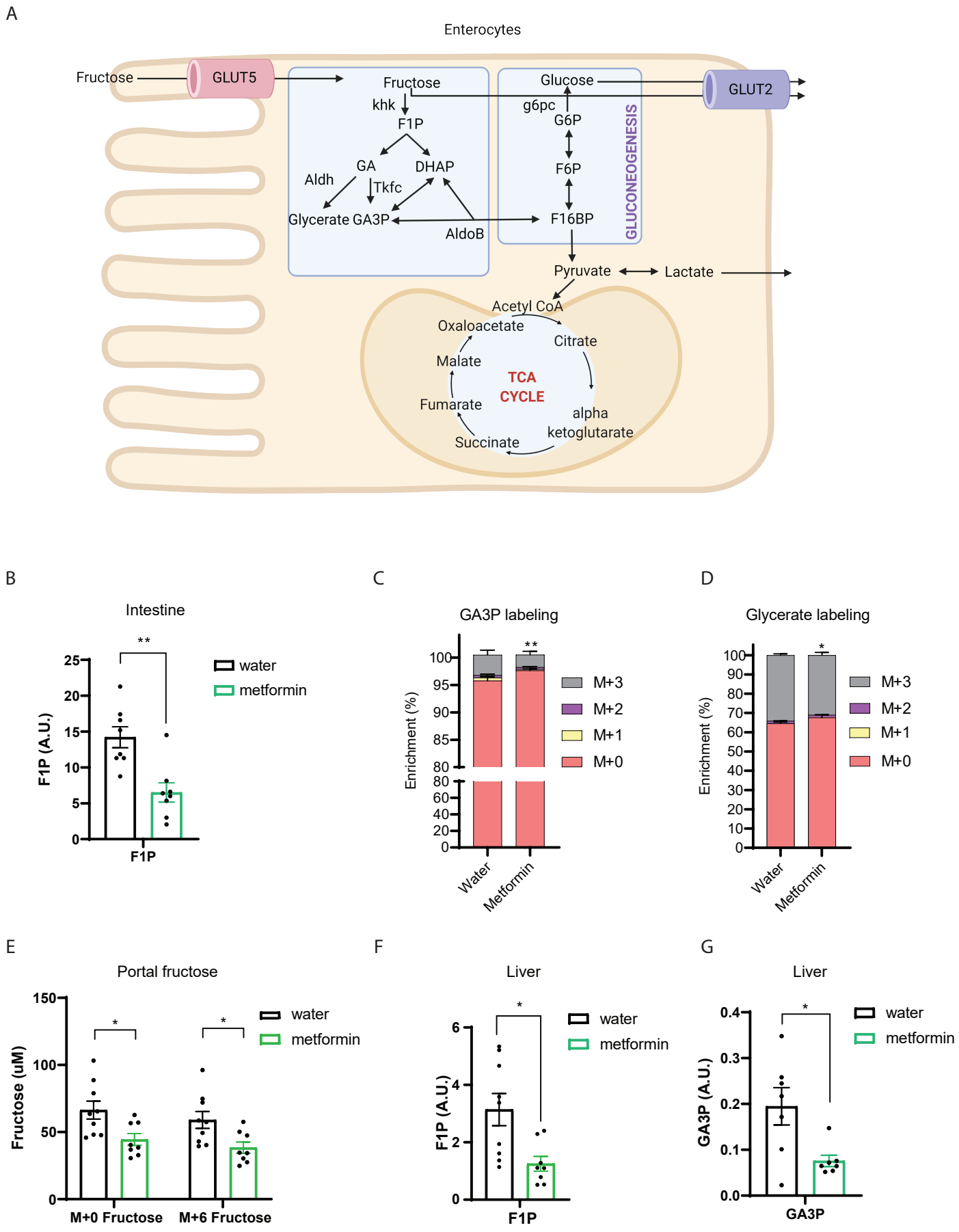
A
Enterocytes
Fructose
GLUT5
Fructose
khk
F1P
GA
DHAP
Aldh
Tkfc
Glycerate GA3P
AldoB
Glucose
g6pc
G6P
F6P
F16BP
GLUCONEOGENESIS
GLUT2
Pyruvate
Lactate
Acetyl CoA
Oxaloacetate
Citrate
Malate
TCA CYCLE
Fumarate
alpha ketoglutarate
Succinate
B
Intestine
F1P (A.U.)
water
metformin
F1P
C
GA3P labeling
Enrichment (%)
M+3
M+2
M+1
M+0
Water
Metformin
D
Glycerate labeling
Enrichment (%)
M+3
M+2
M+1
M+0
Water
Metformin
E
Portal fructose
Fructose (uM)
water
metformin
M+0 Fructose
M+6 Fructose
F
Liver
F1P (A.U.)
water
metformin
F1P
G
Liver
GA3P (A.U.)
water
metformin
GA3P

Figure 3

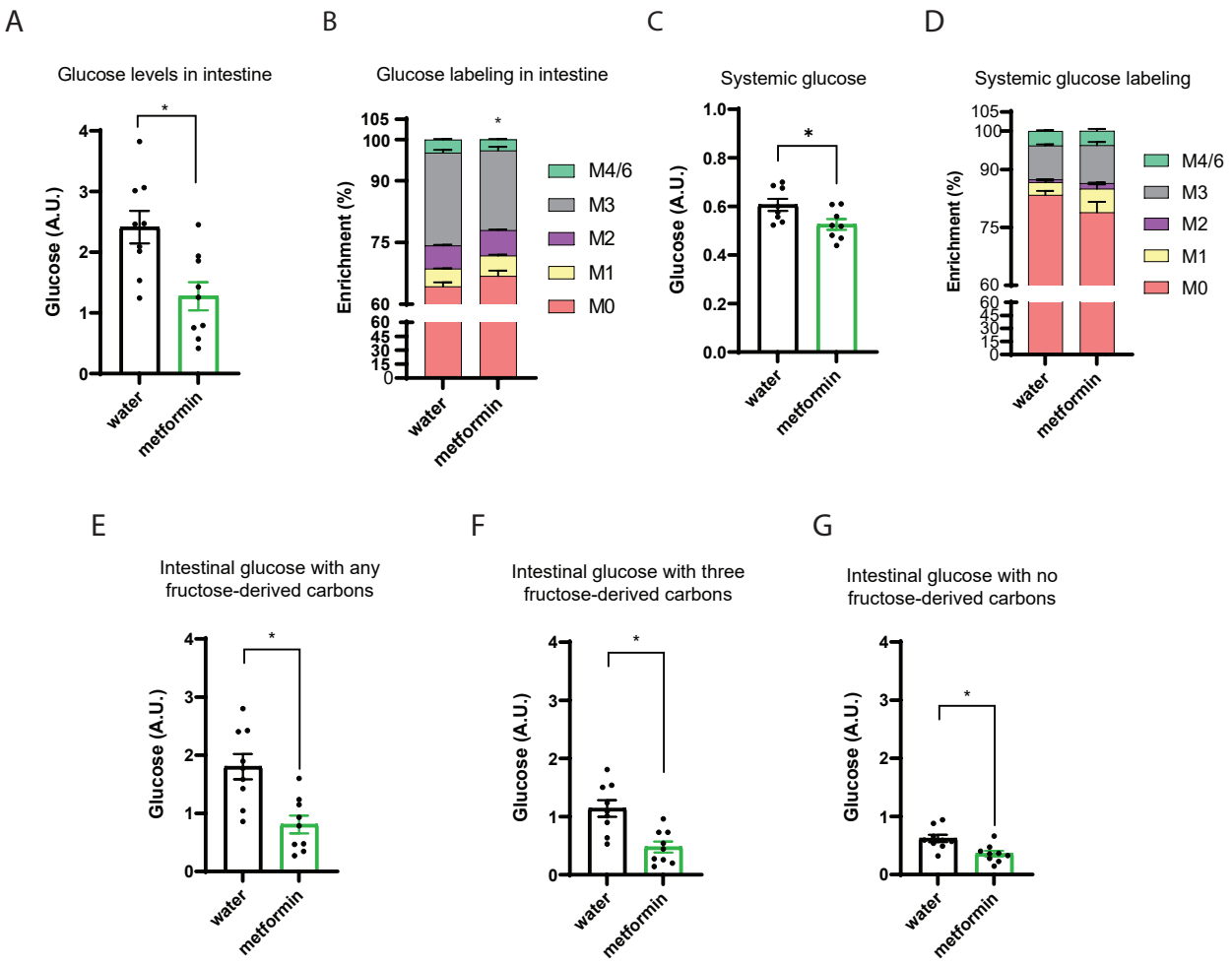
A
Glucose levels in intestine
Glucose (A.U.)
water
metformin
B
Glucose labeling in intestine
Enrichment (%)
M4/6
M3
M2
M1
M0
C
Systemic glucose
D
Systemic glucose labeling
E
Intestinal glucose with any fructose-derived carbons
F
Intestinal glucose with three fructose-derived carbons
G
Intestinal glucose with no fructose-derived carbons

Figure 4

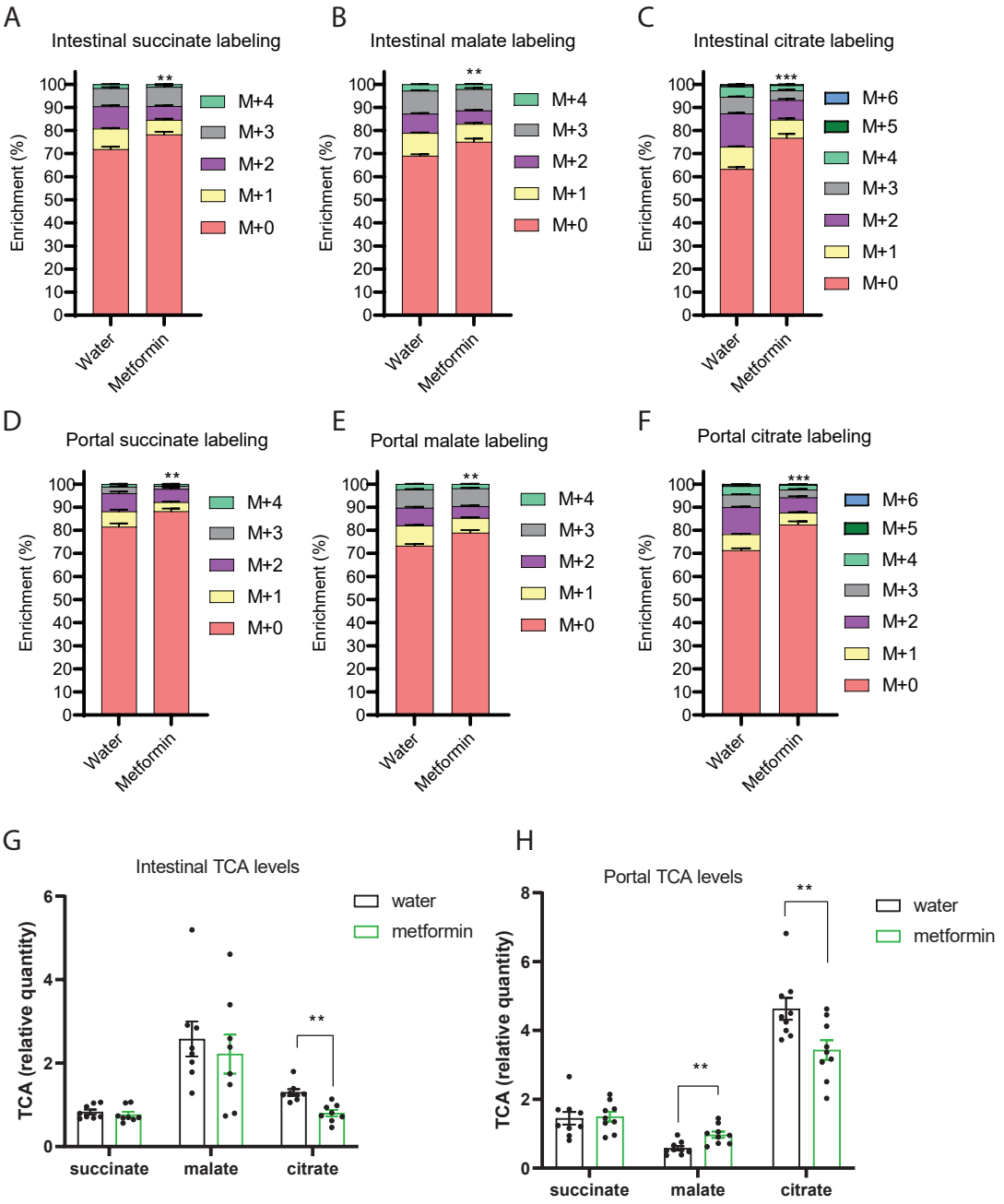
A
Intestinal succinate labeling
B
Intestinal malate labeling
C
Intestinal citrate labeling
D
Portal succinate labeling
E
Portal malate labeling
F
Portal citrate labeling
Enrichment (%)
Water
Metformin
M+6
M+5
M+4
M+3
M+2
M+1
M+0
G
Intestinal TCA levels
H
Portal TCA levels
TCA (relative quantity)
water
metformin
succinate
malate
citrate

Figure 5

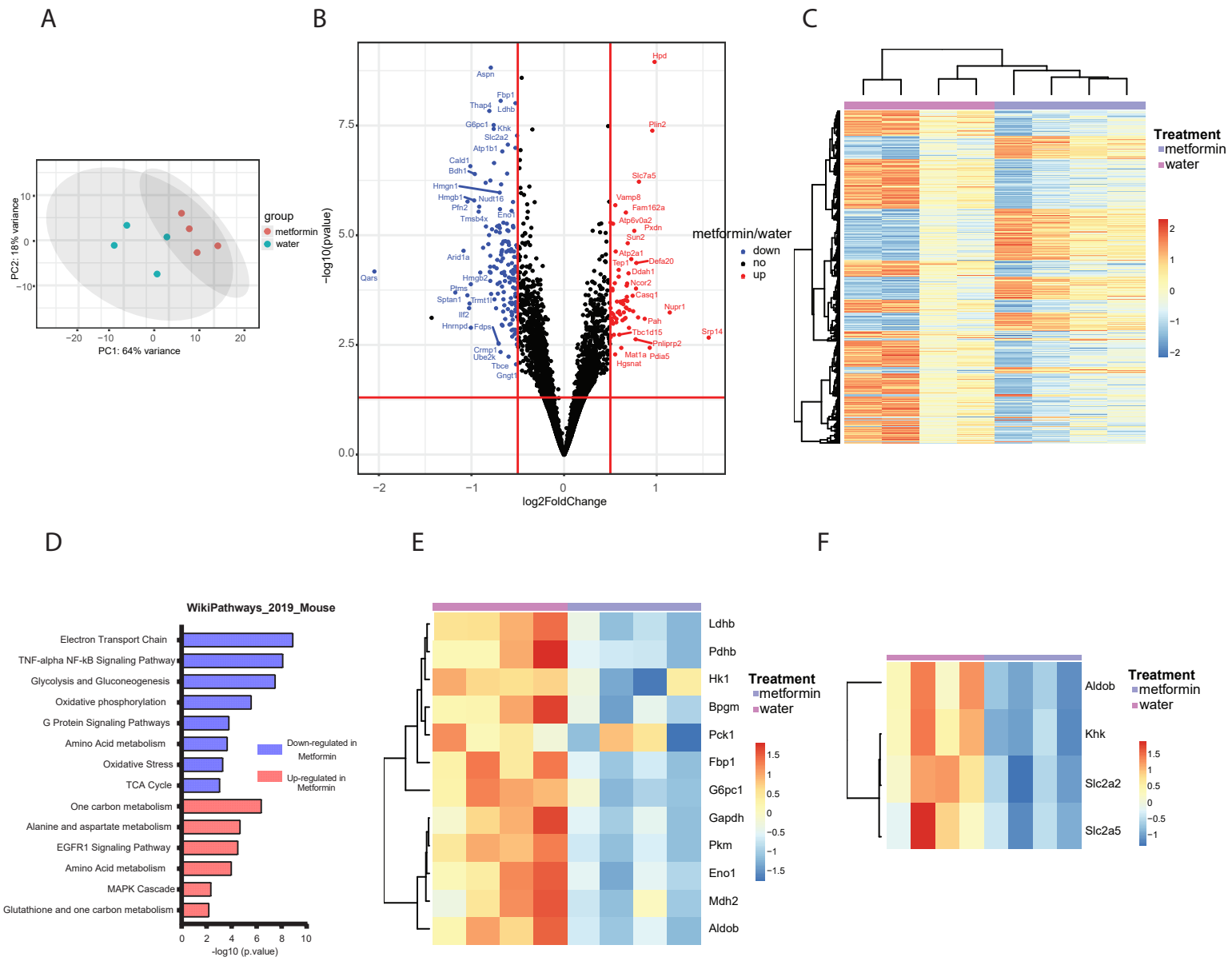
A
PC2: 18% variance
PC1: 64% variance
group
metformin
water
B
−log10(pvalue)
log2FoldChange
metformin/water
down
no
up
Hpd
Aspn
Fbp1
Thap4
Ldhb
G6pc1
Khk
Slc2a2
Atp1b1
Cald1
Bdh1
Hmgn1
Hmgb1
Nudt16
Pfn2
Eno1
Tmsb4x
Arid1a
Qars
Hmgb2
Pfms
Sptan1
Trmt11
Ilf2
Hnrnpd
Fdps
Crmp1
Ube2k
Tbce
Gngt1
Plin2
Slc7a5
Vamp8
Fam162a
Atp6v0a2
Pxdn
Sun2
Atp2a1
Tep1
Defa20
Ddah1
Ncor2
Casq1
Nupr1
Pah
Tbc1d15
Srp14
Pnliprp2
Mat1a
Pdia5
Hgsnat
C
Treatment
metformin
water
D
WikiPathways_2019_Mouse
Electron Transport Chain
TNF-alpha NF-kB Signaling Pathway
Glycolysis and Gluconeogenesis
Oxidative phosphorylation
G Protein Signaling Pathways
Amino Acid metabolism
Oxidative Stress
TCA Cycle
One carbon metabolism
Alanine and aspartate metabolism
EGFR1 Signaling Pathway
Amino Acid metabolism
MAPK Cascade
Glutathione and one carbon metabolism
Down-regulated in Metformin
Up-regulated in Metformin
-log10 (p.value)
E
Ldhb
Pdhb
Hk1
Bpgm
Pck1
Fbp1
G6pc1
Gapdh
Pkm
Eno1
Mdh2
Aldob
Treatment
metformin
water
F
Aldob
Khk
Slc2a2
Slc2a5
Treatment
metformin
water

Figure 6

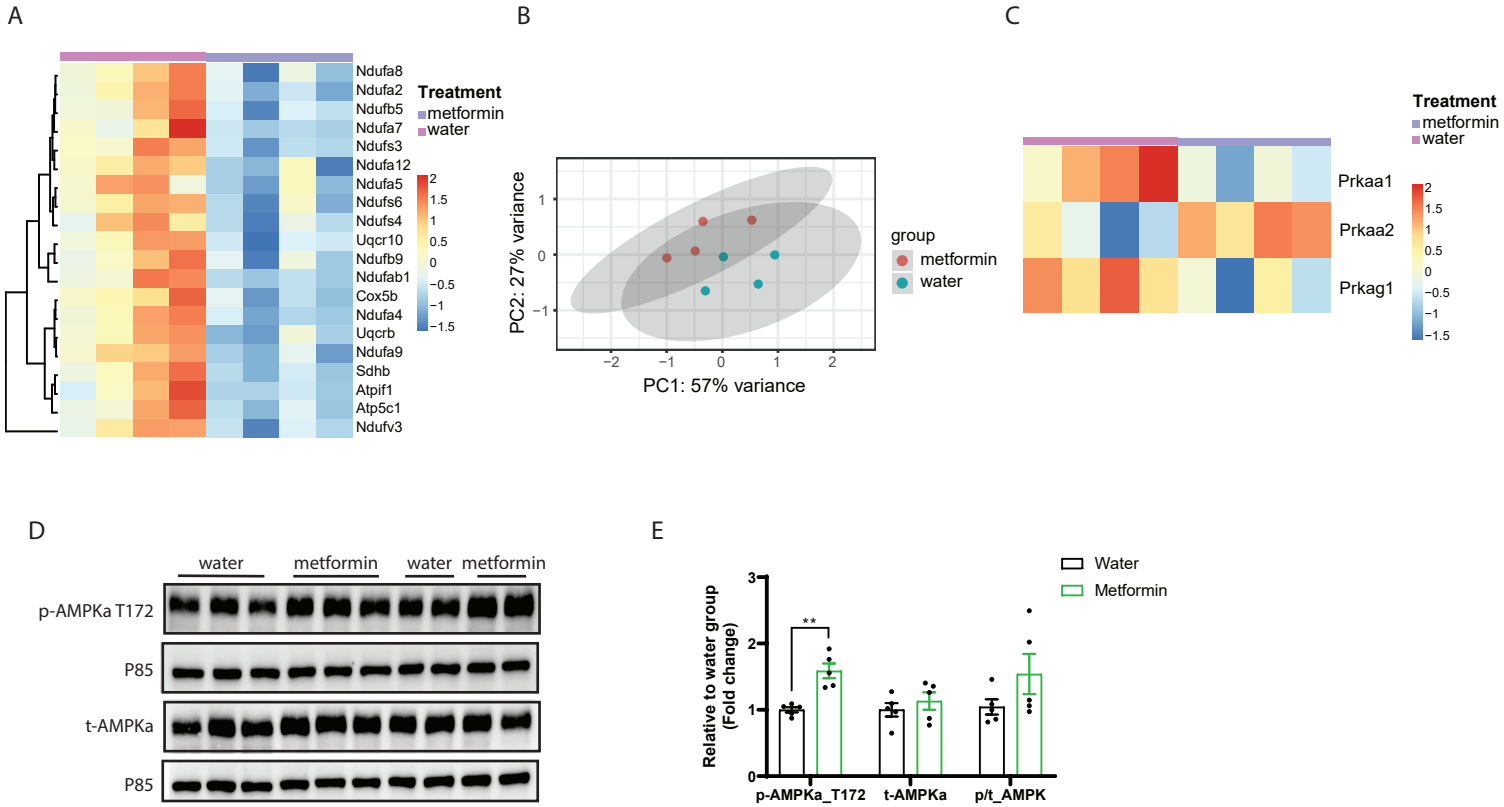
A
Ndufa8
Ndufa2
Ndufb5
Ndufa7
Ndufs3
Ndufa12
Ndufa5
Ndufs6
Ndufs4
Uqcr10
Ndufb9
Ndufab1
Cox5b
Ndufa4
Uqcrb
Ndufa9
Sdhb
Atpif1
Atp5c1
Ndufv3
Treatment
metformin
water
2
1.5
1
0.5
0
−0.5
−1
−1.5
B
PC2: 27% variance
PC1: 57% variance
group
metformin
water
C
Prkaa1
Prkaa2
Prkag1
Treatment
metformin
water
D
water
metformin
water
metformin
p-AMPKa T172
P85
t-AMPKa
P85
E
Water
Metformin
Relative to water group (Fold change)
**
p-AMPKa_T172
t-AMPKa
p/t_AMPK